ELSEVIER

Journal of Fluids and Structures 22 (2006) 345–369

JOURNAL OF FLUIDS AND STRUCTURES

www.elsevier.com/locate/jfs

Flow-induced vibration of a square cylinder without and with interference

R. Ajith Kumar[a,*], B.H.L. Gowda[b]

[a]*Department of Mechanical Engineering, Amrita Vishwa VidyaPeetham (Deemed University), Ettimadai Campus, Coimbatore 641 105 Tamil Nadu, India*

[b]*Department of Applied Mechanics, Indian Institute of Technology Madras, Chennai 36, India*

Received 2 April 2004; accepted 20 November 2005
Available online 10 February 2006

Abstract

This paper presents the results of an investigation on the interference effects of a rigid square cylinder on the transverse vibrations of a spring-mounted square cylinder (test cylinder) exposed to a uniform flow. The interference effects were studied for the tandem, side-by-side and staggered arrangements. Experiments have been carried out for various relative dimensions of the test cylinder and the interfering cylinder; the tests for the staggered arrangements were conducted at several tandem distances between the two. The results indicate that there is a critical combination of relative dimensions and spacing that gives rise to maximum amplitude of vibration. Among the cases studied, tandem arrangement with $L/B = 1.25$ and $b/B = 0.5$ gives rise to maximum amplitude of vibration with $(a/B)_{\max} = 0.57$. A tentative explanation is offered for the observed features based on flow-visualization studies conducted as a part of the experimental investigation.

1. Introduction

When a flexibly mounted body, either streamlined (e.g., an aerofoil) or bluff (e.g., a circular or square cylinder), is exposed to a steady and uniform flow, fluid–structure interactions can take place as a result of which the body can experience fluctuating pressure forces of considerable magnitude causing the body to undergo induced vibrations. Another body or bodies in its vicinity (situated in the flow field) can be expected to alter the magnitude and phasing of pressure fluctuations acting on the body and thereby the induced vibrations. Aerodynamic interference between bodies is found to depend on various factors such as the body geometry, reduced velocity, longitudinal and transverse spacing between them (and hence, on the arrangement) and also on their support conditions [e.g., Bokaian and Geoola (1985), Zdravkovich (1985), Takeuchi (1990), Takeuchi and Matsumoto (1993)].

Literature shows that considerable amount of data are available on the flow-induced oscillations of bodies with circular cross-section, whereas it is found to be limited on prismatic bodies with square and rectangular cross-sections. This is true for the cases with body in isolation and with interference. Interference effects on the flow-induced vibrations of cylindrical bodies with circular cross-section and prismatic bodies with square cross-section are important in many

*Corresponding author. Tel.: +91 422 2656422x362; fax: +91 422 2656274.
E-mail address: ajithkumar_64@yahoo.co.in (R.A. Kumar).

0889-9746/$ - see front matter © 2006 Elsevier Ltd. All rights reserved.
doi:10.1016/j.jfluidstructs.2005.11.006

Nomenclature

a	peak-to-peak amplitude
a'	distance of separation of the test cylinder from the mean position
B	side dimension of the test cylinder
b	side dimension of the interfering cylinder
D	diameter of the test circular cylinder
d	diameter of the interfering circular cylinder
f	fundamental natural frequency of the spring–cylinder system
k_s	Scruton number: mass damping parameter ($2m\delta/pB^2$)
L	longitudinal spacing between axes of cylinders
m	mass per unit length of the test cylinder
T	transverse spacing between axes of cylinders
U	free stream velocity
δ	logarithmic decrement
ρ	density of air

practical situations such as flow around chimney stacks, tube bundles in heat exchangers, power transmission lines, offshore structures, bridge pylons, building structures, etc.

On square cylinders, for the single cylinder case there are enough data, but comparatively less information on cases with interference. The investigations of Vickery (1966), Bostok and Mair (1972), Otsuki et al. (1974), Nakamura and Mizota (1975), Wilkinson (1981), Bearman and Obasaju (1982), Olivari (1983), Sakamoto (1985) and Bearman and Luo (1988) have dealt with single square cylinder cases wherein they have brought out various aerodynamic characteristics and forces acting on a square cylinder. Interference effects between two square cylinders in tandem arrangement were investigated by Blessmann and Riera (1985), Shiraishi et al. (1986), Sakamoto et al. (1987), Luo and Teng (1990) and Takeuchi and Matsumoto (1992, 1993) wherein they have brought out various aerodynamic properties, response characteristics and mechanisms underlying aerodynamic behaviour of square cylinders. Similar aerodynamic characteristics were brought out for square cylinders in side-by-side and staggered arrangements by other investigators (Bailey and Kwok, 1985; Sakamoto and Haniu, 1988; Taniike and Inaoka, 1988; Taniike, 1992).

In the present study, the vibratory response of a spring-mounted square cylinder (test cylinder) due to the interference of another rigid square cylinder (interfering cylinder) placed in tandem, side-by-side and staggered arrangements is described. The results for the test cylinder without interference are first obtained. Then, the interference studies have been carried out at a velocity corresponding to the peak amplitude of the isolated cylinder without interference. In all the cases considered, the interfering cylinder was never upstream of the test cylinder. In an attempt to bring out the influence of geometry, in some of the cases, the results are compared with those of circular geometry (Sreedharan, 1992; Gowda and Sreedharan, 1994). The response of the test cylinder was obtained for different ratios of interfering cylinder side dimension b to the test cylinder side dimension B: i.e., $b/B = 0.5$, 1.0, 1.5 and 2.0 (see Fig. 1).

2. Experimental set-up

2.1. Wind tunnel facility

The arrangement is essentially the same as that used by Gowda and Deshkulkarni (1988) and Gowda and Prabhu (1987), Gowda and Sreedharan, (1994). The experiments were conducted on an aluminium tube with a square cross-section of side 12 mm, wall thickness 1 mm and length 140 mm. The cylinder was positioned vertically at the centre of a rectangular frame supported by four springs. The frame was positioned in front of an open-circuit wind tunnel with a square exit duct measuring 120 mm × 120 mm such that the cylinder was at a distance of 44 mm from the exit of the tunnel. The velocity is uniform over the 70% of the exit cross-section (variation is less than 1%) and reduces gradually towards the edges.

One of the springs supporting the cylinder was connected to a dynamic pick up (Type 8001; Brüel and Kjaer). The pick up was in turn connected to a storage oscilloscope (Type 1744A; Hewlett Packard) through a charge amplifier (Type 2626; Brüel and Kjaer). The cylinder was capable of vibrating in a direction transverse to the oncoming flow. The natural frequency and the logarithmic decrement of the spring-mounted cylinder were determined to be 54 Hz and 0.00368, respectively. The mass damping parameter k_s (Scruton number) was equal to 3.2 (see Nomenclature).

The interfering cylinders used for tandem and staggered arrangement were made out of solid aluminium rods with a smooth finish and square cross-section. They were each of length 140 mm and side dimension ratios (b/B) of 0.5, 1.0, 1.5

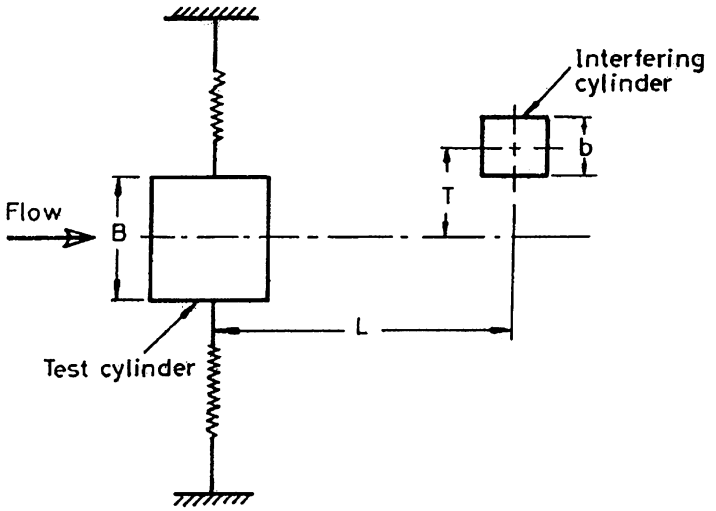

Fig. 1. The configuration tested. Cases studied: $b/B = 0.5$, 1.0, 1.5 and 2.0.

and 2.0 were used. For the side-by-side arrangement, a different set of cylinders of the same relative dimensions as for the tandem and staggered arrangements were used. These cylinders were 120 mm long and could be conveniently placed besides the test cylinder. Further details of the wind tunnel test set-up have been given by Gowda and Prabhu (1987). However, the test set-up is given here for the sake of clarity, in Figs. 2(a)–(d). The response of the test cylinder without any interference was first determined. Then, the interference studies were carried out by considering various interference cases constituting tandem, side-by-side and staggered arrangements. The range of Reynolds number referred to the test cylinder side dimension is between 3000 and 11 000.

2.2. *Flow visualization facility*

The flow-visualization experiments are carried out for two situations: (a) with two stationary cylinders and (b) with one cylinder oscillated and the other cylinder stationary. These are carried out in a recirculating water channel shown in Fig. 3. It consists of a tank 2.5 m × 1.5 m with a depth of 150 mm, at one end of which are located two sets of aluminium discs (vanes) with suitable spacing between them. When these vanes are rotated, they act as paddles and create a flow that is suitably guided to the test-section where the models are placed. A variable speed DC motor is used for rotating the vanes and a fairly wide range of flow speeds can be achieved in the test-section. The fluid in the tank is water and fine aluminium powder is used as tracer medium.

In situation (a), corresponding to the test cylinder in air experiments, the cylinder employed is a square rod with side dimension 30 mm. Interfering cylinders are also square rods with $b/B = 0.5$, 1.0, 1.5 and 2.0. Experiments are conducted at a Reynolds number of 5200. This is the Reynolds number corresponding to the velocity at the maximum amplitude of the test cylinder under isolated condition in air experiments. The spacing ratios L/B and T/B are systematically varied for each value of b/B and the flow patterns are photographed by mounting an SLR Pentax camera at a suitable location above the models. Proper lighting is obtained by using halogen lamps.

For situation (b), where the vibration of the test cylinder is also simulated, additionally an arrangement has been made to make one of the cylinder oscillate in the water channel, as shown in Fig. 4. Considerable effort was required for the design and fabrication of this arrangement (Fig. 4). Basically, the rotary motion provided by a variable speed DC motor is converted into a translatory to-and-fro motion (oscillation) utilizing a cam arrangement specially designed and made for the purpose. The cam arrangement (Fig. 4) consists of a slotted circular disc made of aluminium, which is screwed tightly to the shaft of the DC motor, so that it rotates with the motor. In the slot made on the circular disc (Fig. 4; side view of cam), a sliding block made of aluminium is provided which can have sliding motion radially. This is achieved by means of a long screw provided as shown in the side view of the cam. To the sliding block, a connecting link (made of a flat piece) is attached which converts the rotary motion of the cam to translatory to-and-fro motion. This translatory motion of the connecting link is transferred to a long sliding rod provided in the system on to which the

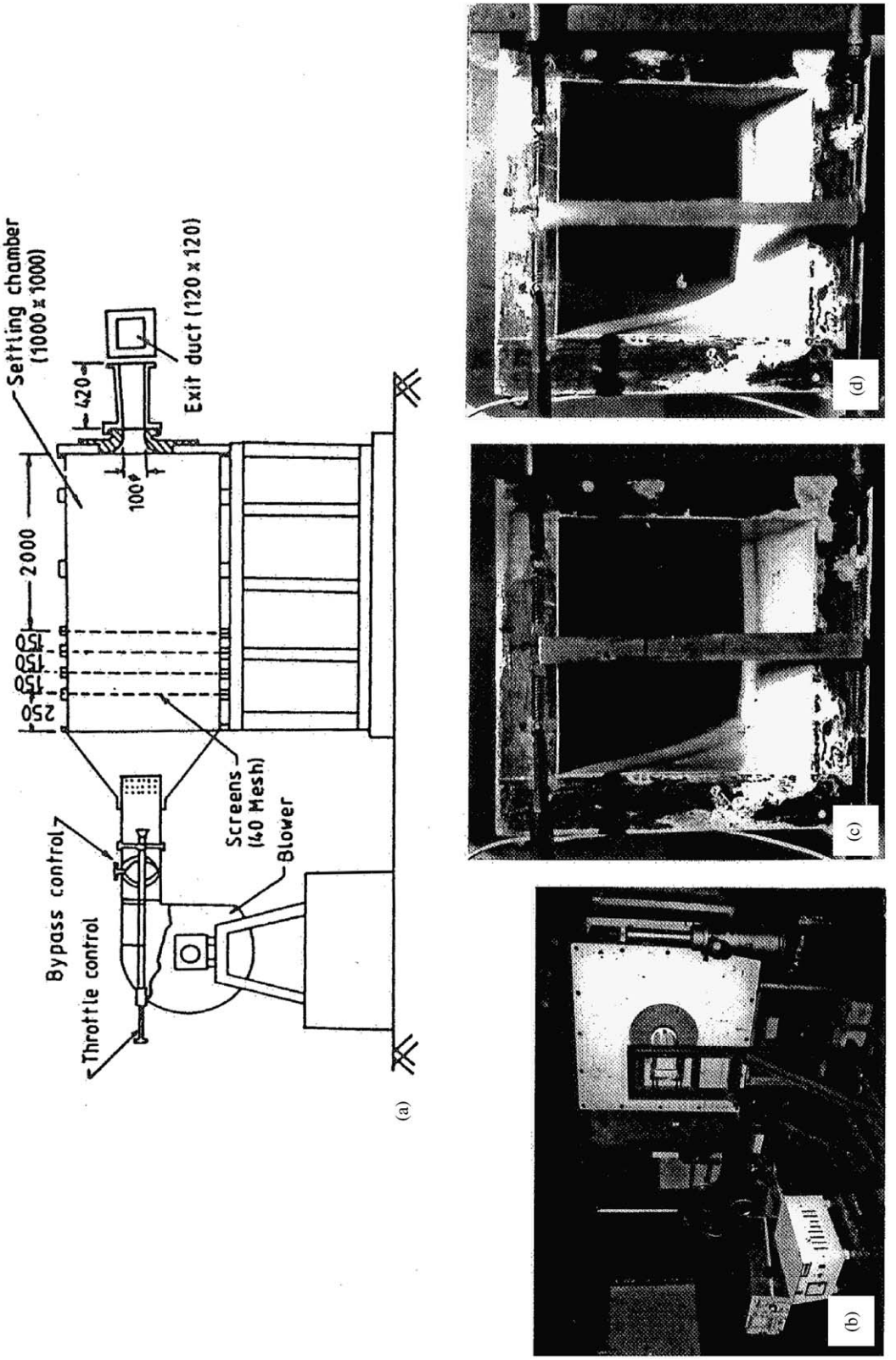

Fig. 2. Experimental set-up: (a) sketch of wind tunnel (dimensions in mm), (b) instrumentation, (c) test cylinder, at rest and (d) test cylinder, vibrating.

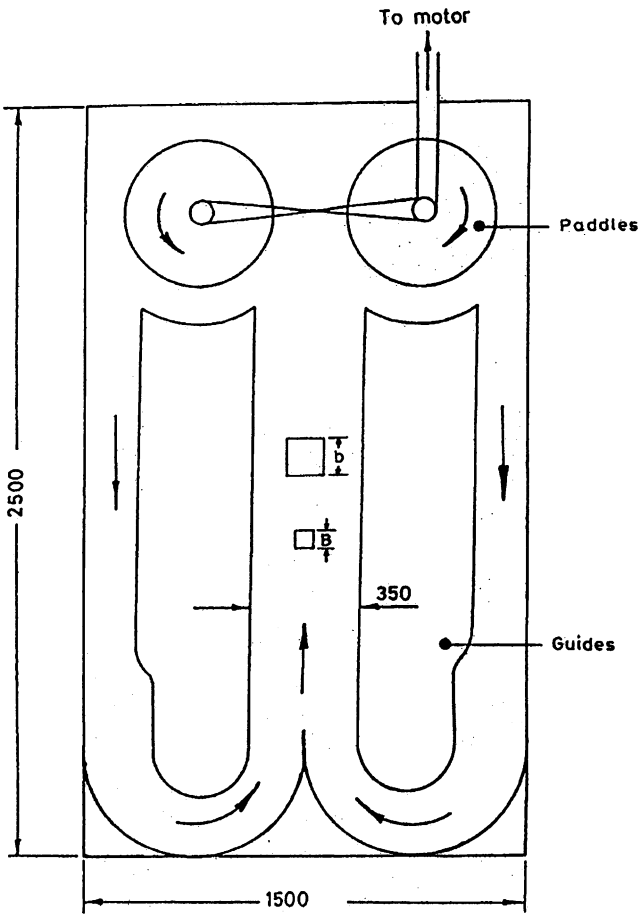

Fig. 3. Schematic view of the flow-visualization tank.

square cylinder is mounted and screwed tightly. The sliding rod passes through three guides (with circular cross-section), which arrests the lateral movements of the rod: one guide with its support system immediately follows the connecting link and the other two guides with their support system follow after the cylinder, as shown in Fig. 4. These guides are welded to their respective support systems.

The amplitude of vibration of the cylinder can be varied by suitably adjusting the position of the sliding block (in the cam) along the screw and fixing it at the desired position using the nuts provided. The frequency can be varied by varying the speed of the DC motor. Thus, the cylinder (simulating the test cylinder in the air experiments) can be made to oscillate with different amplitudes and frequencies in the water channel. Suitable adjustments are made in the position of the motor and the model, so that the model would oscillate about the mid-point of the channel.

The direction of motion of the test cylinder is sensed with the help of an electric circuitry made (Fig. 4), comprising of a battery and a light-emitting diode (LED). The LED is 'on' when the test cylinder moves in a particular direction and 'off' when it moves in the other direction. To achieve this, a make-and-brake arrangement has been made in which a metallic pointer is made to rub against the cam surface as it rotates. Half the surface area of the cam is covered with an insulation tape over a section of the width which comes in contact with the metallic pointer. Hence, as the cam rotates, the pointer rubs against the surface making the circuit closed for half the rotation; i.e., for half the cycle of oscillation of the test cylinder and the LED will be 'on'. The circuit will be open for the other half of the rotation, where the LED will be 'off'. To make the glow of LED to be properly seen in the presence of the intense luminous field of the halogen lamps, it is encased in a centrally holed rubber ball as shown in the figure (Fig. 4).

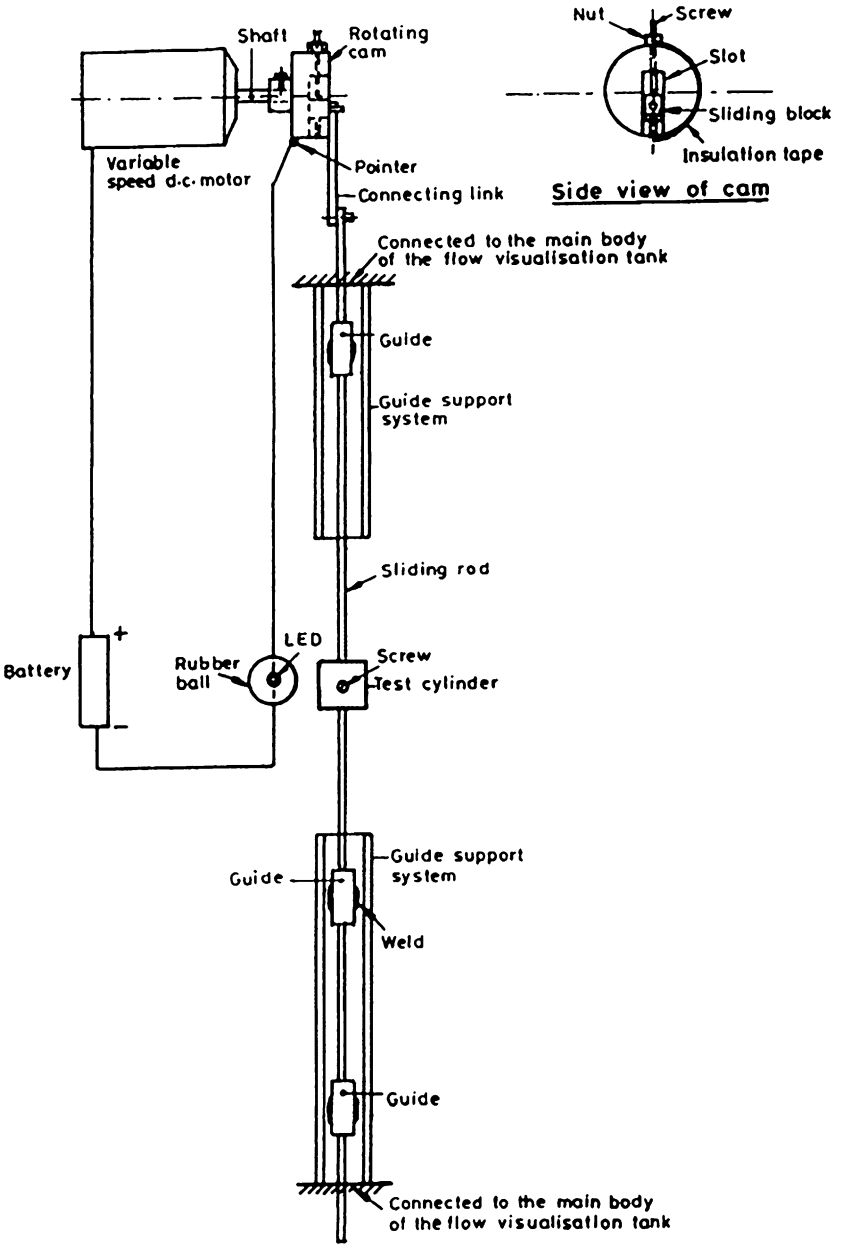

Fig. 4. Schematic view of the vibrating set-up in flow-visualization.

3. Results and discussion

3.1. Single cylinder

Before carrying out the interference studies, the response of the test cylinder without any interfering body is obtained and is shown in Fig. 5. In this figure, the variation of the nondimensional amplitude (a/B) with reduced velocity (U/fB) is plotted. Results have been obtained with velocity increasing and decreasing. It is seen from Fig. 5 that vortex lock-in starts at a reduced velocity (U/fB) of 7.3. This corresponds to a Strouhal number of 0.137, which is in very good agreement with the values obtained by other investigators (Bearman et al., 1987; Okajima, 1990; Lyn et al., 1995).

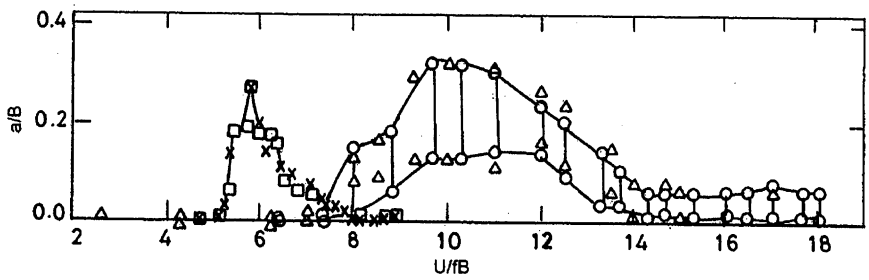

Fig. 5. The response of the test cylinder without interference: O, velocity increasing, Δ, velocity decreasing (square cylinder); □, velocity increasing and x, velocity decreasing (circular cylinder; Gowda and Sreedharan, 1994).

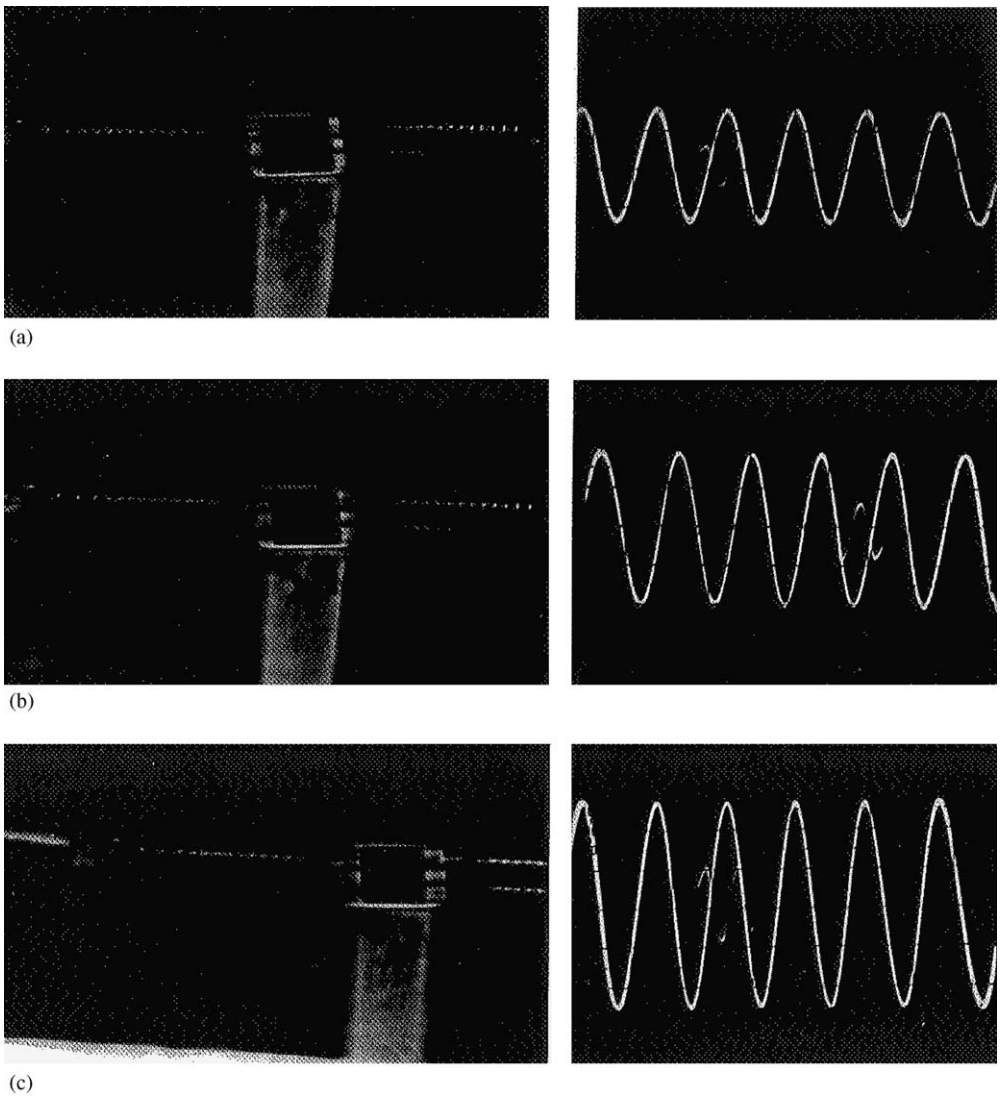

Fig. 6. Test cylinder executing multiple amplitudes: (a) minimum amplitude, (b) intermediate amplitude and (c) maximum amplitude.

The resonance range observed is $7.3 \leqslant U/fB \leqslant 14.0$ with a peak value of amplitude of vibration, $(a/B)_{\max}$ of 0.32. The maximum amplitude remains nearly the same over a small range of reduced velocities between 9.6 and 11.0. The lock-in ceases at a reduced velocity of 14.0. The amplitude of vibration is negligibly small to the left of the "resonance hill" and relatively small to the right of it. Hysteresis is found to be negligible, as seen in Fig. 5. A very interesting feature noticed in the vibratory response of the test cylinder is its multiple amplitudes within a low and a high peak, as depicted in Fig. 5. The (square) test cylinder amplitude was observed to vary from a minimum to a maximum value, sometimes having a halt at an intermediate amplitude position from where it goes to the maximum amplitude position and vice versa. Some other times, it varies from the minimum amplitude position to the maximum without any intermediate halt. There was no regular frequency noticed in the above-mentioned switch from one amplitude level to the other. What is shown in Fig. 5 is the minimum and the maximum values of vibration amplitudes reached. Fig. 6 shows the photographs of the test cylinder vibrating, when it assumes the minimum, an intermediate and the maximum amplitudes. The reduced velocity (U/fB) considered in Fig. 6 is 10.0, which corresponds to the maximum amplitude of vibration of the test cylinder (Fig. 5).

The resonance range obtained is comparable to that observed by Bearman and Obasaju (1982). They have observed that the reduced velocity range corresponding to vortex resonance is $7.0 \leqslant U/fB \leqslant 12.0$, with the maximum nondimensional amplitude of vibration value of 0.25 for a square-section cylinder. However, they have not reported the multiple amplitudes as observed in the present study. This might be due to the difference in the value of Scruton number and the other experimental conditions between the investigations.

The response curve for an isolated circular cylinder (Gowda and Sreedharan, 1994) is also included in Fig. 5 for comparison. It is very interesting to observe the differences in the nature of the response between the two. The resonance for the circular cylinder starts at around a reduced velocity of 5 (as the Strouhal number is around 0.2), whereas it begins at a value of $U/fB = 7.3$ (Strouhal number = 0.137) for the square cylinder. The lock-in region for the square section is wider with higher peak amplitude of oscillation; also, there is a flatter peak. The other major difference is the multiple amplitudes observed for the square cylinder, unlike for the circular one. The reason for such a vibratory response (i.e., the multiple amplitudes of vibration) of the square cylinder can be explained as follows.

For the square cross-section, unlike for the circular geometry, while in vibration, the influence of change in the effective angle of flow incidence on the flow field around the cylinder can be expected to be considerable. The configuration of the shear layers separating from the sharp corners of the square section continuously change (Obasaju, 1983). Laneville and Lu (1983) have argued that the change in the configuration of shear layers would bring about changes in the characteristics of the flow separation bubble and its interaction with the vortex formation process. Out of such complex interaction between the flow separation bubble and the vortex formation process, there is a possibility that multistable flow conditions could prevail around the square cylinder due to which an abrupt amplitude switch from one level to the other could occur, leading to a vibratory motion with multiple amplitudes as observed in the present case.

Further supportive argument is provided by Luo et al. (1994) in which they have dealt with the change in the configuration of shear layers (with respect to the corresponding sides) as the square cylinder vibrates. This leads to variations in the suction forces generated on the side surfaces and hence, in the vibrations. Fig. 7 of the paper by Parkinson (1971) typically shows the pressure variation brought about by the change in the position of the shear layers (top and bottom) with respect to the corresponding sides due to the change in the flow angle of incidence. However, the explanations given for the occurrence of multiple amplitudes are of tentative nature and the exact reasons for the observed behaviour is yet to be understood.

3.2. Interference effects at a particular velocity

As mentioned earlier, the interference effects have been obtained at a velocity corresponding to the peak amplitude of the isolated cylinder, without interference. The reduced velocity for this is $U/fB = 10.0$. At this reduced velocity, studies have been carried out for tandem, side-by-side and staggered arrangements. Flow visualization results have also been obtained using two rigid cylinders for various interference positions: (a) when both of them are stationary, (b) when one of them is oscillated (to simulate the vibrations of the test cylinder observed in wind tunnel experiments) and the other is stationary. The vibratory response of the test cylinder is first described and then, an explanation for the observed trends is given. In all the cases, $b/B = 0.5$, 1.0, 1.5 and 2.0 are considered. It is to be mentioned that the frequency of vibration of the test cylinder with interference remains the same as that for the isolated case, i.e., 54 Hz. This was determined and checked by the signals in the oscilloscope.

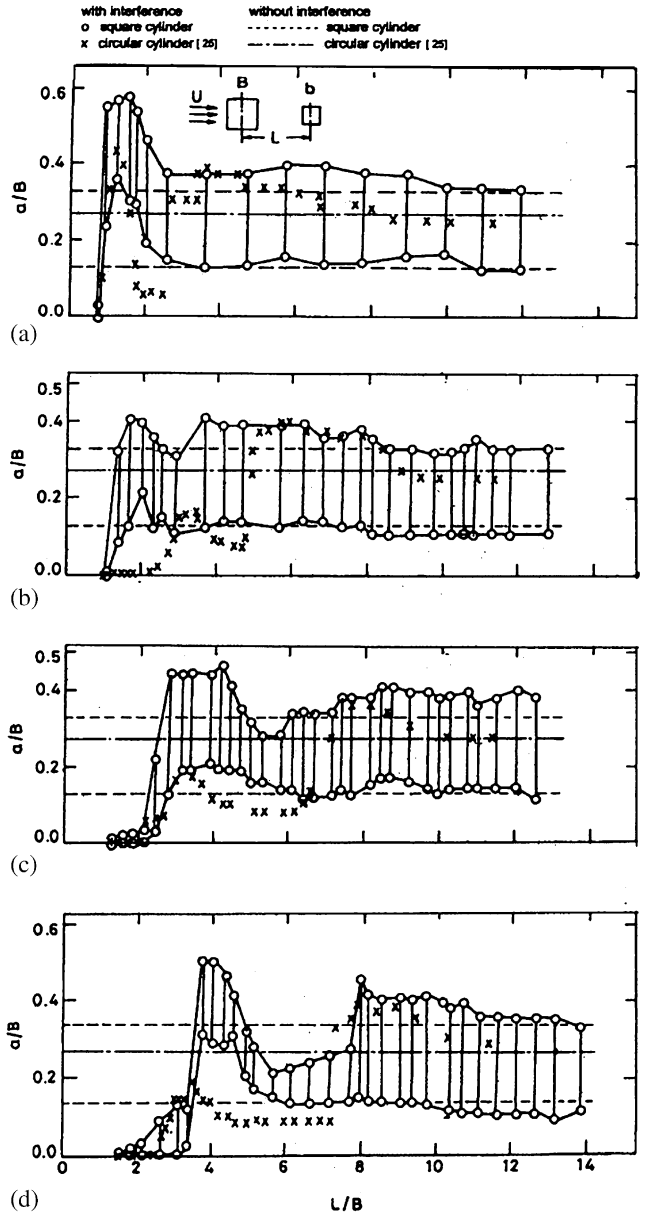

Fig. 7. Interference effects for tandem arrangement ($U/fB = 10.0$): (a) $b/B = 0.5$; $d/D = 0.5$, (b) $b/B = 1.0$; $d/D = 1.0$, (c) $b/B = 1.5$; $d/D = 1.5$ and (d) $b/B = 2.0$; $d/D = 2.0$.

3.2.1. Oscillatory response

3.2.1.1. Tandem arrangement. In all the interference studies, the test cylinder is allowed to oscillate steadily at a reduced velocity of 10.0 and then the interfering cylinder is introduced. In the case of tandem arrangement, the longitudinal spacing ratio (L/B) is reduced gradually in small steps from a very large value where, the interference effects are negligible. The results for the tandem arrangement are presented in Fig. 7. The results for circular cylinder (Sreedharan, 1992) are also included for comparison, in an attempt to reveal the effect of body geometry. It is to be noted that the Scruton number for the circular cylinder (Sreedharan, 1992) is very nearly the same as that of the square cylinder ($k_s = 3.25$ for circular cylinder; $k_s = 3.20$ for the square cylinder). In this figure, the amplitude levels for the no-interference case for both the circular and square cylinders are also shown (dotted lines for square cylinder and

chain-line for circular cylinder). In what follows, the results obtained are first described and then an explanation for the observed trends is given towards the end of the section. In all the cases of interference, the multiple amplitudes of oscillation are observed as in the case of isolated cylinder response (Fig. 5).

Considering the case of $b/B = 0.5$ (Fig. 7(a)), it is seen that as the interfering cylinder approaches the test cylinder, the amplitude gradually increases with the effects becoming noticeable for $L/B \leqslant 10.0$. There is a sudden increase in the amplitude at around $L/B = 2.6$, reaching the maximum amplitude of vibration at around $L/B = 1.5$ ($(a/B)_{max} = 0.57$) and the amplitude steeply decreases to negligible values at around $L/B = 1.0$.

The response of the test cylinder for $b/B = 1.0$ (Fig. 7(b)) is different from that of $b/B = 0.5$, in that the interference effects are felt at much larger spacing (up to $L/B = 14.0$). A sudden drop of amplitude occurs at around $L/B = 3.0$ with a peak amplitude around $L/B = 2.0$, after which amplitude steeply decreases as shown in the figure.

The response of the test cylinder for $b/B = 1.5$ is shown in Fig. 7(c). Interference effects are felt at much larger spacing in this case also. There is a sudden decrease in amplitude at around $L/B = 6.0$, after which amplitude increases and reaches a peak plateau of amplitude. The maximum amplitude of vibration ($(a/B)_{max} = 0.45$) remains constant in the range $3.0 \leqslant L/B \leqslant 4.2$. The amplitude of vibration is completely suppressed for $L/B \leqslant 2.0$. The response of the test cylinder for $b/B = 2.0$ (Fig. 7(d)) is similar to that for $b/B = 1.5$ (Fig. 7(c)), but with some distinctive differences. In the range of spacing $6.0 \leqslant L/B \leqslant 8.0$, the amplitude of vibration was observed to be partially suppressed. There is a sharp major peak of amplitude observed at around $L/B = 4.0$, whereas in the case of $L/B = 1.5$, the maximum amplitude extends over a range. Unlike all the other b/B ratios, for $b/B = 2.0$ a second minor peak is observed at around $L/B = 3.0$ with much reduced amplitude of vibration. The amplitude of vibration seems to come down to negligible levels almost linearly in the range $2.0 \leqslant L/B \leqslant 3.0$.

Considering the response of the square cylinder with that of the circular cylinder, it is seen that the response of the latter at $d/D = 0.5$ (Fig. 7(a)) is similar to that for square cylinder, except that there is a minor dip of amplitude occurring at around $L/D = 3.5$ and a major dip at around $L/D = 2.75$. Similar to square cylinder, there is a sharp peak of amplitude observed at around $L/D = 1.25$. In general, the vibratory amplitude levels for the circular cylinder are lower than that of the square cylinder. Furthermore, no multiple amplitudes are observed for the circular cylinder, unlike the case of the square cylinder.

For $d/D = 1.0$ and 1.5 (Figs. 7(b) and (c)), for circular cylinder, the positions of the sudden decrease of amplitude and that of minor peak occur at larger spacing when compared to the square cylinder. In the case of $d/D = 1.0$ (Fig. 7(b)), for $L/D \leqslant 2.0$, vibrations are completely suppressed for the circular cylinder, whereas it is not so for the square cylinder; the maximum amplitude of vibration is almost the same for both square and circular cylinders. In the case of $b/B = 1.5$ (Fig. 7(c)), the square cylinder exhibits higher amplitudes (than the circular cylinder) throughout the range of spacing tested. For $b/B = 2.0$, the features observed, such as the position of peak amplitudes and sudden drop of amplitude, and the general vibratory trend are nearly similar for both square and circular cylinders. The maximum amplitude is considerably higher for the square cylinder (Fig. 7(d)).

Fig. 8 shows the photographs of the test cylinder vibrations (maximum amplitudes) at a reduced velocity (U/fB) of 10.0, in the tandem position with $L/B = 2.5$ and $T/B = 0$ for all the b/B ratios.

3.2.1.2. Side-by-side arrangement. The results for the side-by-side arrangement are shown in Fig. 9(a)–(d), for $b/B =$ 0.5 to 2.0, respectively. The experiments were conducted by placing the interfering cylinder beside the test cylinder as close as possible, such that there was no hindrance to the oscillations of the latter. The interfering cylinder was moved away from the test cylinder in small steps.

The response of the test cylinder for $b/B = 0.5$ (Fig. 9(a)) is seen to be different from other cases, in that a minor peak is observed at $T/B = 1.0$ and the vibrations are completely suppressed at $T/B = 1.25$. Beyond this value, the amplitude increases rapidly and reaches the no-interference value at around $T/B = 2.0$; the amplitudes are unaltered for $T/B > 2.5$. For other values of b/B (Fig. 9(b)–(d)), there is an initial range of T/B (which is nearly the same for all the three cases) where the vibrations are suppressed. Then, there is a steep build-up in amplitudes with their magnitudes reaching the no-interference value over a short range of T/B. The interference effects are negligible for $T/B > 3.0$. The multiple amplitudes (as mentioned in the case of single cylinder case) persist with interference also. Another feature observed is that the amplitude levels reached in the experiments with interference, even at large values of T/B, can be slightly different from the levels for the single cylinder case; either slightly less as in the case of $d/B = 0.5$ (Fig. 9(a)) or slightly more as in the case of $b/B = 1.5$ and 2.0 (Fig. 9(c) and (d)). In general, this can also be attributed to the sensitiveness of the square shape to the changing effective angle of incidence in its vibration cycle.

Comparing the results of the square cylinder with those of the circular cylinder, it is seen that there is a basic difference in the response of the former. Multiple amplitudes are observed for the square cylinder, whereas it is not so for the circular one. But, in spite of this basic difference, some similarities can be observed between the two. It can be seen that the response characteristics of square and circular cylinders are similar in trend, for $b/B = 1.5$ and 2.0

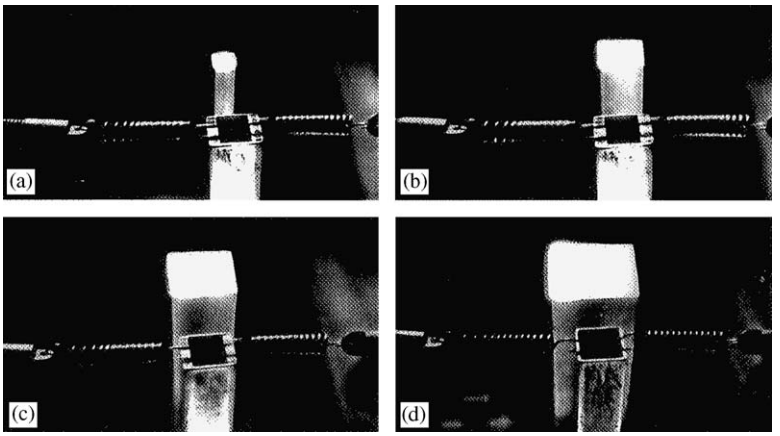

Fig. 8. Test cylinder vibrations, with interference: $L/B = 2.5$, $T/B = 0$; $U/fB = 10.0$: (a) $b/B = 0.5$, $(a/B)_{max} = 0.37$, (b) $b/B = 1.0$, $(a/B)_{max} = 0.34$ (c) $b/B = 1.5$, $(a/B)_{max} = 0.23$, and (d) $b/B = 2.0$, $(a/B)_{max} = 0.08$.

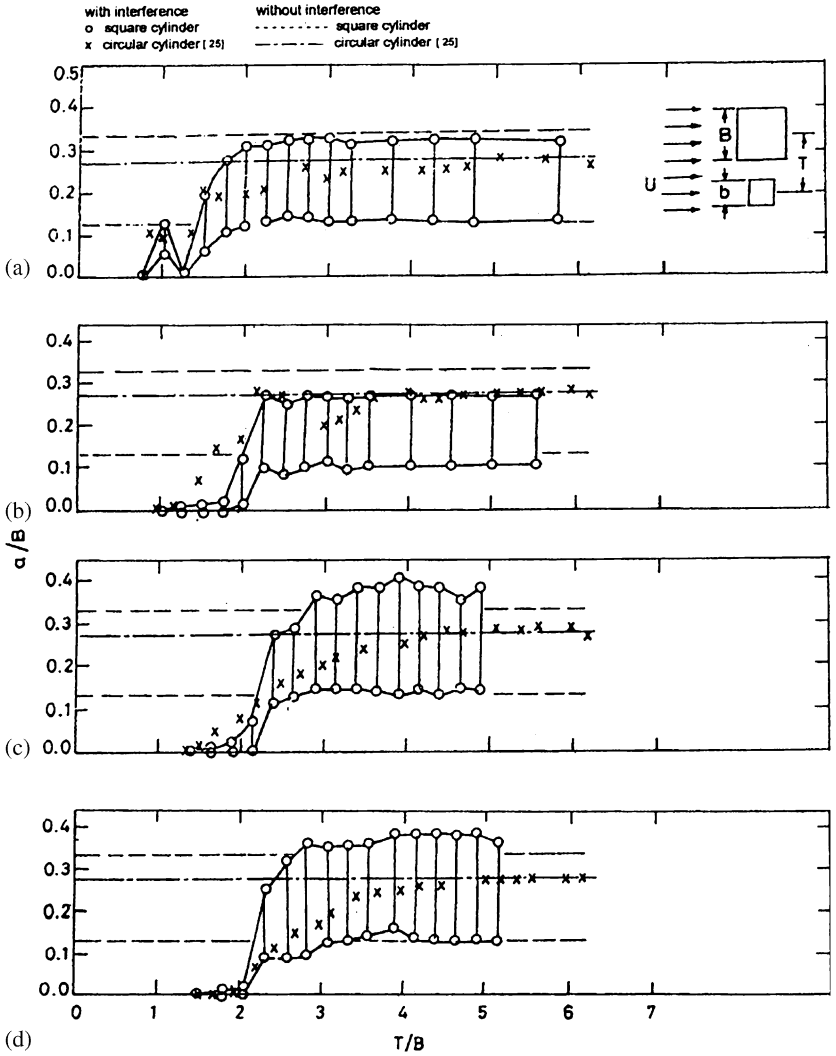

Fig. 9. Interference effects for side-by-side arrangement ($U/fB = 10.0$): (a) $b/B = 0.5$; $d/D = 0.5$, (b) $b/B = 1.0$; $d/D = 1.0$, (c) $b/B = 1.5$; $d/D = 1.5$ and (d) $b/B = 2.0$; $d/D = 2.0$.

(Fig. 9(c) and (d)). However, for $b/B = 1.5$, the spacing range of amplitude suppression is greater for the square cylinder (extending up to $T/B = 2.0$), whereas it is only up to $T/D = 1.5$ for the circular cylinder. In general, for the circular cylinder, interference effects become negligibly small for $T/D > 4.0$; whereas, for the square cylinder, this occurs for $T/B > 3.0$. For $b/B = 0.5$ and 1.0, the amplitude variation trend of the square cylinder considerably differs from that of the circular cylinder ($d/D = 0.5$ and 1.0) as Figs. 9(a) and (b) show. In general, with the same interference conditions, the amplitude levels are higher for the square cylinder when compared to the circular cylinder, as seen in Fig. 9.

3.2.1.3. Staggered arrangement. The interference effects in the staggered arrangement were studied by positioning the interfering cylinder downstream of the test cylinder at particular values of L/B (which were chosen based on the results shown in Fig. 7) and moving it transverse to the flow in small steps. The experiments were carried out by considering a few positions on one side of the tandem position and several positions on the other. The few positions considered on one side are in order to test for consistency (symmetry of readings) about the tandem position, $T/B = 0$.

The first set of experiments were carried out for the case with $b/B = 0.5$ and $L/B = 1.25$, 5.0 and 10.0 and the results are shown in Fig. 10(a)–(c). For $L/B = 1.25$ (Fig. 10(a)), it is seen that when the interfering cylinder is slightly moved from its tandem position, the vibration of the test cylinder is drastically reduced and gets suppressed at around $T/B = 1.5$. With further increase in T/B, the amplitude increases, and beyond $T/B = 3.0$, the interference effects are negligible. At $L/B = 5.0$ (Fig. 10(b)), some interference effects are noticed for $0 \leqslant T/B \leqslant 1.5$ (increasing–decreasing amplitude trend), and beyond $T/B = 1.5$, interference effects are negligible. At $L/B = 10.0$, the interference effects are negligibly small as seen in Fig. 10(c).

The results for $b/B = 1.0$ are shown in the set of Fig. 11(a)–(d). In this case also, the positions chosen are with reference to Fig. 7. At $L/B = 1.8$ (Fig. 11(a)), when the test cylinder is displaced slightly from the tandem position ($T/B = 0$), the amplitude levels drastically come down, ending up in a vibration suppression region with $0.75 \leqslant T/B \leqslant 2.0$. With further increase in T/B, the amplitude steeply increases up to $T/B = 2.5$ and then gradually

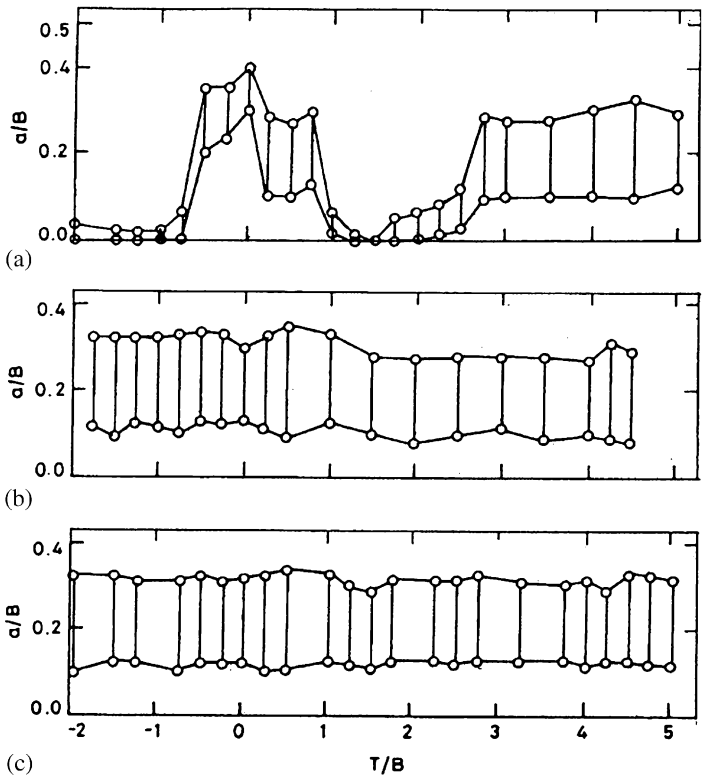

Fig. 10. Interference effects for staggered arrangement: $b/B = 0.5$; $U/fB = 10.0$: (a) $L/B = 1.25$, (b) $L/B = 5.0$ and (c) $L/B = 10.0$.

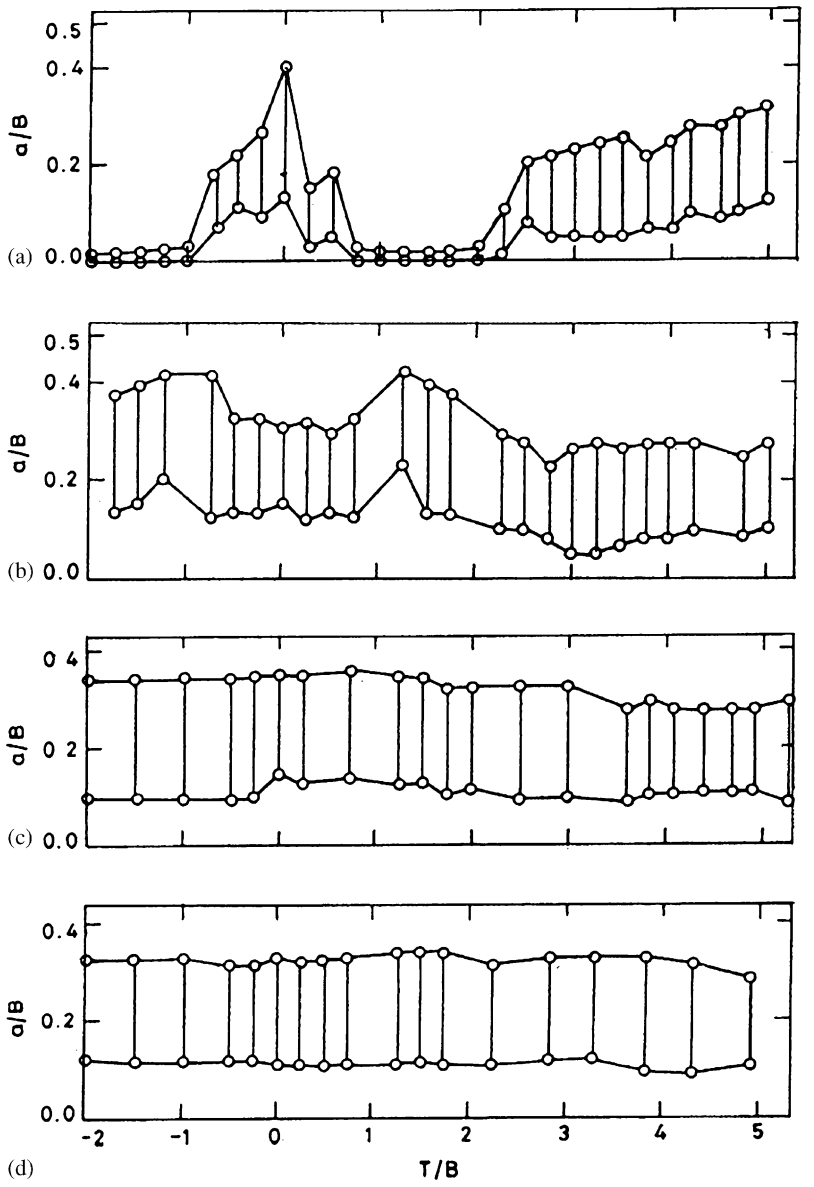

Fig. 11. Interference effects for staggered arrangement: $b/B = 1.0$; $U/fB = 10.0$: (a) $L/B = 1.80$, (b) $L/B = 3.0$, (c) $L/B = 5.0$ and (d) $L/B = 10.0$.

reaches the no-interference value at around $T/B = 5.0$. At $L/B = 3.0$ (Fig. 11(b)) also, considerable interference effects can be noticed within the range $0 \leqslant T/B \leqslant 3.0$. As the test cylinder is moved away from the tandem position, amplitude steeply increases (beyond $T/B = 0.5$) at first up to $T/B = 1.25$, followed by a continuous decrease up to $T/B = 2.75$. Beyond $T/B = 2.75$, interference effects are negligible. At $L/B = 5.0$ and 10.0, interference effects are not significant (Figs. 11(c) and (d)).

The results for $b/B = 1.5$ at $L/B = 3.5$, 5.5 and 10.0 are shown in Fig. 12(a)–(c) and the results for $b/B = 2.0$ at $L/B = 4.0$, 6.0, 8.0 and 11.0 are shown in Figs . 13(a)–(d). The variations are clear to see from these figures.

Among all arrangements considered, the tandem arrangement was found to give rise to maximum amplification of vibratory amplitudes. For the tandem arrangement (Fig. 7), the location and magnitude of the peak amplitude with b/B ratios at the test reduced velocity, viz. $U/fB = 10.0$ are shown in Figs. 14 and 15. It could be seen that due to interference effects, higher the b/B ratio, larger the L/B value at which major peak occurs (Fig. 14) and among all the b/B ratios, that maximum amplification of vibratory amplitude occurs for $b/B = 0.5$ (Fig. 15).

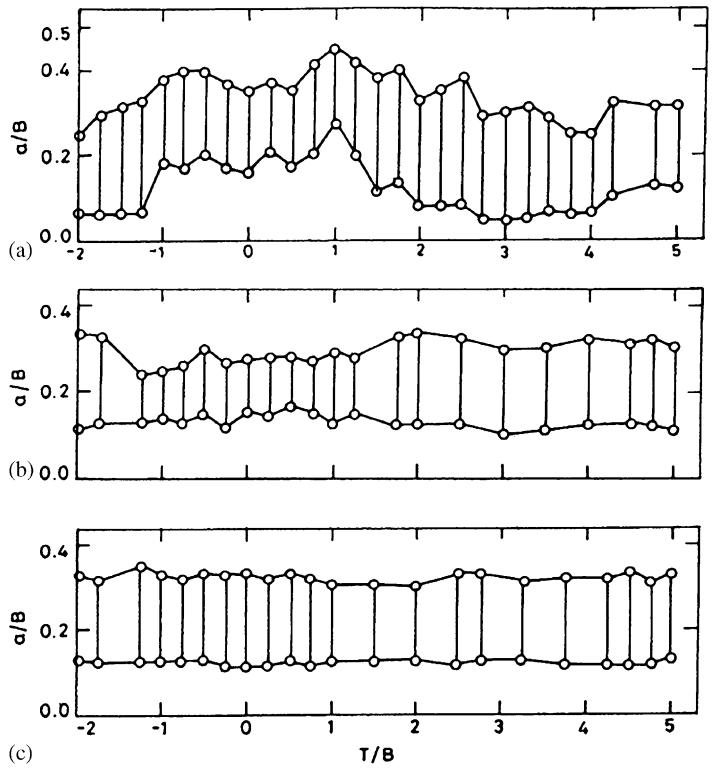

Fig. 12. Interference effects for staggered arrangement: $b/B = 1.5$; $U/fB = 10.0$: (a) $L/B = 3.50$, (b) $L/B = 5.5$ and (c) $L/B = 10.0$.

All interference cases for the present investigation are presented at a reduced velocity value of 10.0. At this reduced velocity, as explained earlier, the test cylinder in its isolated condition would come under vortex excitation. With interference, except that due to the presence of the interfering cylinder (depending on the size ratio and relative position) the magnitude of vibrations have undergone a magnification or suppression as the case may be, basically, the oscillations could be expected to occur only under vortex resonance.

With interference also, multiple amplitudes are observed similar to the case of the isolated cylinder. The explanation for the case of the single cylinder is already given in Section 3.1. With interference, in addition to the complexities explained earlier, the interfering cylinder is seen to lead a flow field which further enhances or strengthens the occurrence of multiple amplitudes. The separating shear layers from the test cylinder during its oscillation cycle are further influenced by the presence of the interfering cylinder. This feature i.e., the change in the orientation of the shear layers from the test cylinder, is brought out in the flow visualization results which are described in the next section.

3.2.2. Flow visualization results

The flow visualization experiments were performed using two rigid cylinders under two conditions: (a) when both are stationary and (b) when one of them is oscillated at frequency equal to the Strouhal frequency, i.e., the synchronization case (with $f_e/f_o = 1.0$, where f_e is the excitation frequency applied to the cylinder, and f_o is the Strouhal frequency), the other cylinder being stationary. In case (b), the nondimensional maximum peak-to-peak amplitude was maintained the same as that of the maximum peak-to-peak value observed in the corresponding interference condition in the air experiments. In case (a), the cylinder which corresponds to the test cylinder in the air experiment is stationary. A large amount of data were obtained for case (a). These results did explain the observed vibratory response of the test cylinder at some relative positions of the interfering cylinder. However, in many other situations, it was not possible to get a clear understanding of the observed features. In order to better simulate the vibratory experimental conditions in the flow-visualization studies, the rigid cylinder that corresponds to

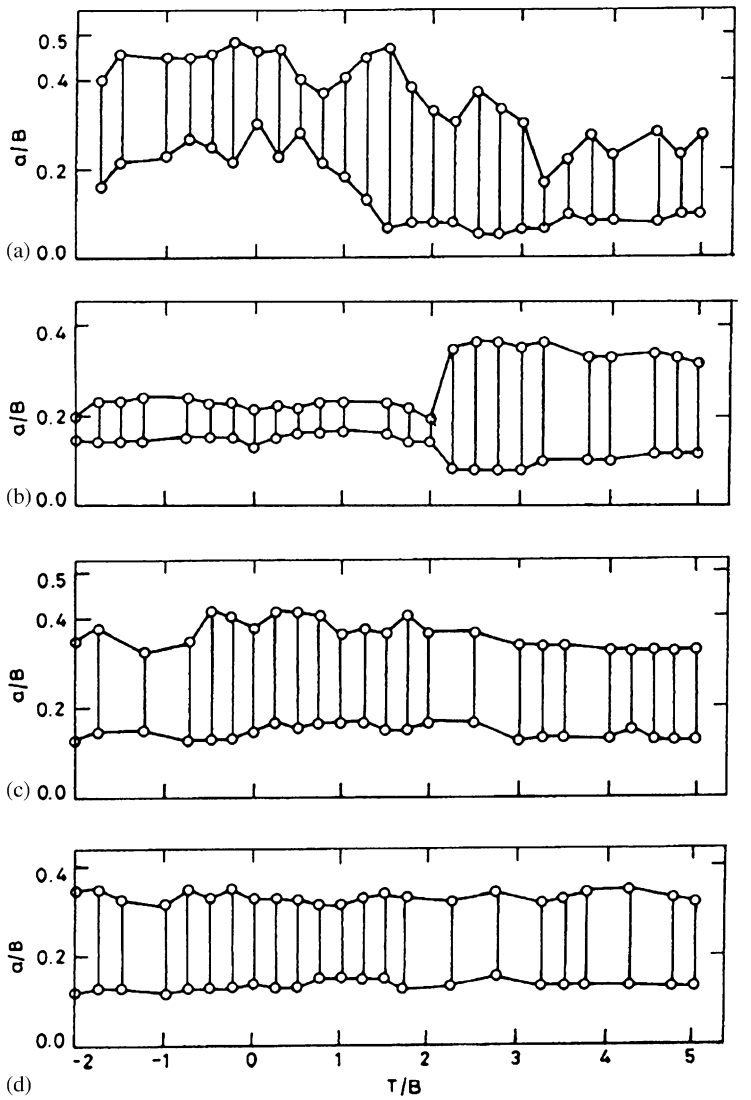

Fig. 13. Interference effects for staggered arrangement: $b/B = 2.0$; $U/fB = 10.0$: (a) $L/B = 4.0$, (b) $L/B = 6.0$, (c) $L/B = 8.0$ and (d) $L/B = 11.0$.

the test cylinder was oscillated as at (b). The interfering cylinder was rigid as in the vibratory (air) experiments. While presenting the flow-visualization results, both the results obtained under conditions (a) and (b) are presented, compared and discussed along with the vibratory response of the test cylinder.

In all the flow-visualization photographs with oscillated cylinder (i.e., case (b)), the small triangular light on the left-hand side indicates that when 'on', the direction of motion of the test cylinder is A' to B' (upward direction), and when 'off', it indicates that the direction of motion is B' to A' (downward direction). These directions are shown in the left-hand side of the photograph in the results presented in the following section. The Reynolds number in all the flow-visualization experiments is 5200 (the same as that at the maximum amplitude of the test cylinder in its isolated condition; Fig. 5). The flow is from left to right. Flow-visualization results are obtained at the same Reynolds number, maximum peak-to-peak amplitude and Strouhal number as that of the air experiments.

To put the interference effects in proper perspective, flow fields around a single square cylinder are captured in stationary and vibrated conditions and are given in Fig. 16(a) and (b).

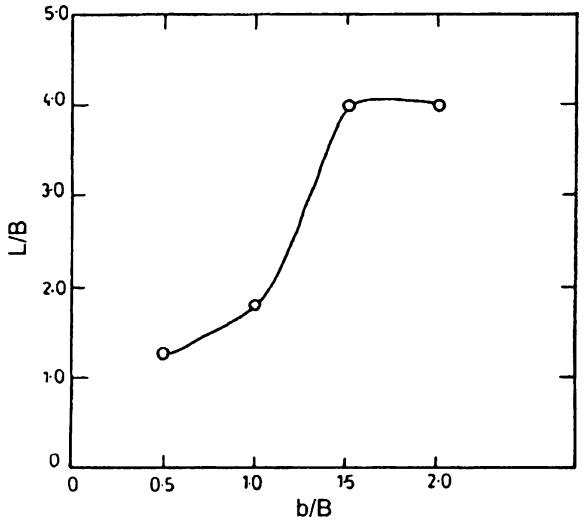

Fig. 14. Position of major peak for different size ratios, at $U/fB = 10.0$ (tandem arrangement).

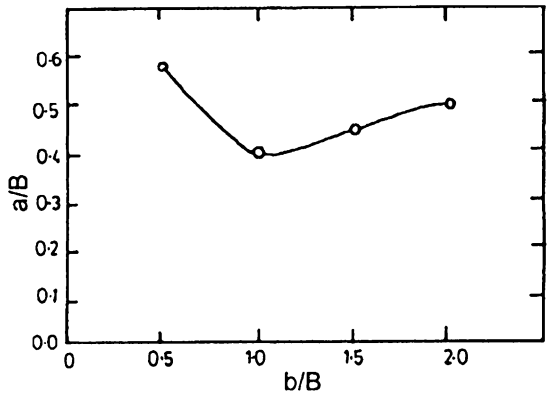

Fig. 15. Amplitudes of the major peak for different size ratios, at $U/fB = 10.0$ (tandem arrangement).

3.2.2.1. Tandem arrangement. Fig. 17 shows the flow patterns for the tandem position with $L/B = 1.25$ and $b/B = 0.5$. At this position, the test cylinder in air experiments experiences very vigorous vibration with $(a/B)_{max} = 0.57$. Considering Fig. 17(a), where both the cylinders are rigid and stationary, it is observed that the smaller cylinder does interfere with the vortex shedding process from the front cylinder (see also Fig. 16(a)). Consequently, one can expect reduced lift force on the front cylinder compared to that for the isolated cylinder. However, it is found that the test cylinder vibrates very vigorously at this position. Hence, the flow-visualization results with a stationary front cylinder (Fig. 17(a)) is not able to explain the vibratory response of the test cylinder. The flow-visualization result at Fig. 17(b) is for the identical position as in Fig. 17(a), but with the front cylinder being oscillated. Under this condition, it is observed that there is vigorous rolling up of shear layers around the front cylinder, indicating strong periodic forces on it. This is reflected in the vibratory experiment with the test cylinder responding with high amplitude. The results in Fig. 17(c) and (d) and in Fig. 17(e) and (f) show the flow patterns at two other positions of the front cylinder in its oscillatory path; Fig. 17(c) and (d) are at $a'/B = 0.18$ and Fig. 17(e) and (f), at $a'/B = 0.23$ (where a' is the distance of separation of the front cylinder from the mean vibratory position). Each set is, for example, Fig. 17(c) and (d) are for the same position but with the front cylinder moving in opposite directions, i.e., A' to B' or B' to A'. It is clear from the patterns shown for each set that the flow fields are quite different for the same position but with different approach direction (A' to B' or B' to A'). Hence, it can be conjectured that the flow field and the relative position of the

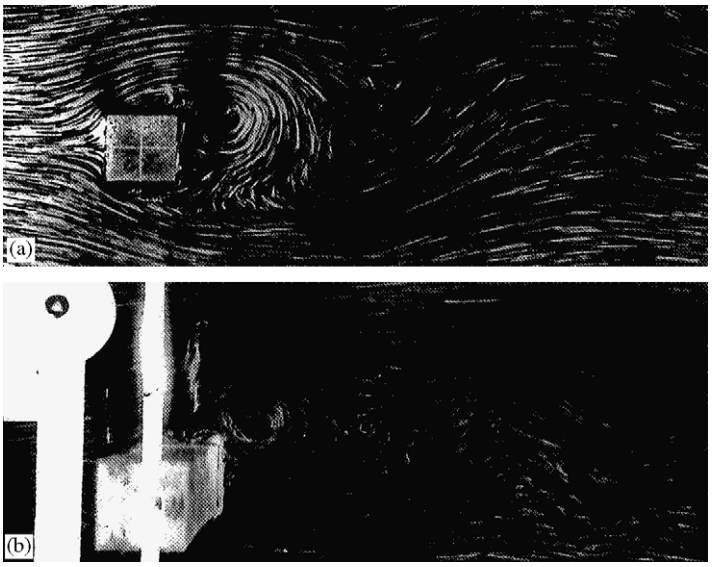

Fig. 16. Typical flow patterns around a square cylinder (Re = 5200): (a) stationary cylinder and (b) oscillated cylinder.

shear layers continuously change as the test cylinder oscillates. This may lead to very complex interaction in the energy feedback mechanism.

Basically, when a cylinder vibrates under vortex excitation, there is a feedback mechanism between the body and the wake (Bishop and Hassan, 1964). Due to the presence of the interfering body, the flow pattern and the vortex shedding phenomenon from the test cylinder can be expected to be altered, which also influences the feedback mechanism; with the result that the test cylinder oscillations vary for different relative positions of the test cylinder and the interfering cylinder. The flow-visualization photographs (Fig. 17(b) to (f)) give the indication that substantial changes occur in the flow field of a vibrating cylinder, as it occupies different displacement positions during its vibration cycle. Also, they indicate that the flow field around a vibrating cylinder can be distinctly different from that of a stationary cylinder (Fig. 17(a)) at the same interference location. Figs. 17(b)–(f) also depicts the change in the configuration of shear layers as the cylinder executes its oscillatory cycle which could ultimately lead to multi-stable flow conditions around the test cylinder (as explained in Section 3.1), if it is elastically mounted as in the case of air experiments. However, in the flow-visualization experiments conducted, the test cylinder is oscillated at definite amplitude (maximum peak-to-peak) and frequency (Strouhal frequency).

For $b/B = 1.0$, at very close spacings, considerable interference effects on the vibratory response are felt (Fig. 7(b)). Typically, at $L/B = 1.8$ and $T/B = 0$, there is a major peak amplitude of vibration observed: $(a/B)_{\max} = 0.42$ (higher than that for single cylinder case for which $(a/B)_{\max} = 0.32$). The flow-visualization results at this position are presented in Fig. 18, which corresponds to the mean vibratory position of the front cylinder when it is moving in the direction A' to B' (cylinder motion, upwards as viewed). In this case, rolling up of shear layers can be observed, indicating strong periodic forces acting on the cylinder which is reflected in the significant response amplitude value observed.

For $b/B = 1.5$, interference effects felt are higher than that for $b/B = 0.5$ and 1.0 (Fig. 7(c)). The maximum amplitude of vibration is observed for a range of spacing $3.0 \leqslant L/B \leqslant 4.2$ with $(a/B)_{\max} = 0.45$ (considerably higher than the single cylinder value of $(a/B)_{\max} = 0.32$). Typically at $L/B = 3.5$ and $T/B = 0$, for $b/B = 1.5$, the flow patterns are as shown in Fig. 19 (where the front cylinder, when it is oscillated, occupies the mean vibratory position). The near wake of the oscillated front cylinder shows intense rolling up of shear layers. This is indicative of considerable lift force on the front cylinder and is reflected in the vibratory response of the test cylinder.

For the size ratio $b/B = 2.0$, at the interference location with $L/B = 4.0$ and $T/B = 0$, the flow patterns are as shown in Fig. 20. The test cylinder in air experiments experiences vigorous vibrations at this position with $(a/B)_{\max} = 0.5$. In Fig. 20(a), where both the cylinders are rigid and stationary, the nearwake of the front cylinder exhibits regular vortex shedding. Hence, the cylinder can be expected to be triggered to notable amplitudes by the periodic forces acting on it. Fig. 20(b) shows the flow pattern around the upstream cylinder, when it is oscillated occupying an identical position as at Fig. 20(a). In Fig. 20(b), intense rolling up of the shear layers is observed. This can give rise to considerable lift force that would act on the front cylinder and is reflected in the vibratory response of the test cylinder.

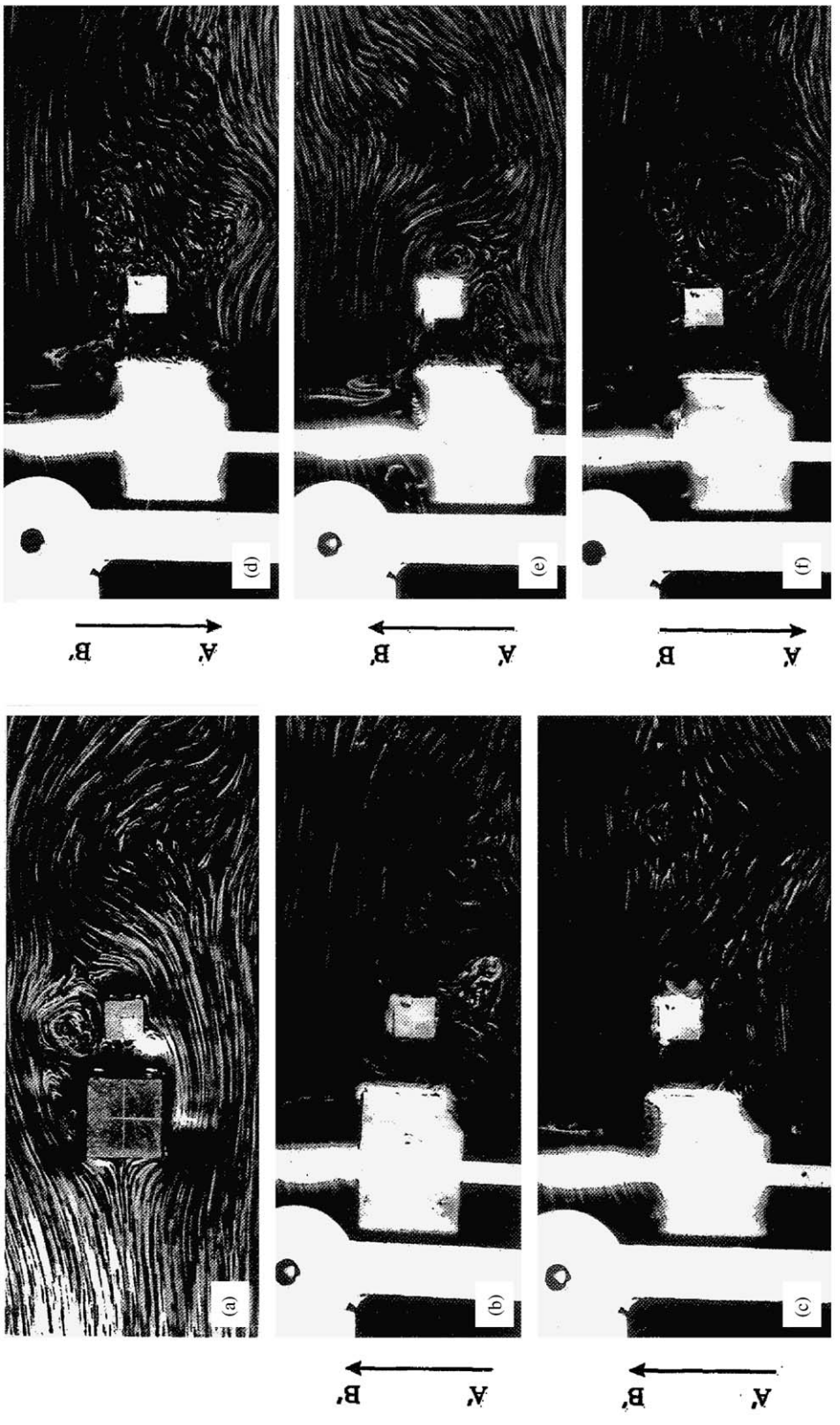

Fig. 17. Typical flow patterns: $L/B = 1.25$, $T/B = 0$; $b/B = 0.5$, $(a/B)_{max} = 0.57$; Re = 5200: (a) stationary front cylinder, (b) oscillated front cylinder at the mean position (dir. $A'B'$), (c) oscillated front cylinder at the intermediated amplitude position ($a'/B = 0.18$ from the mean position; dir. $A'B'$), (d) oscillated front cylinder at the intermediate amplitude position. ($a'/B = 0.18$ from the mean position; dir. $B'A'$), (e) oscillated front cylinder at the intermediate amplitude position ($a'/B = 0.23$ from the mean position; dir. $A'B'$) and (f) oscillated front cylinder at the intermediate amplitude position ($a'/B = 0.23$ from the mean position; dir. $B'A'$).

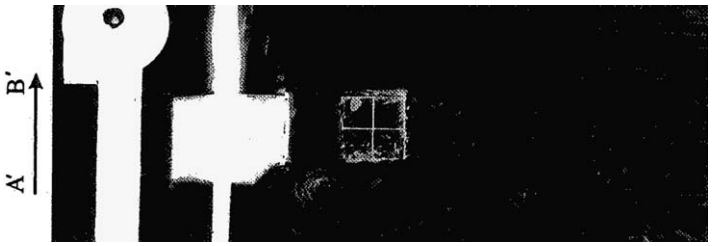

Fig. 18. Typical flow pattern: $L/B = 1.80$, $T/B = 0$; $b/B = 1.0$, $(a/B)_{max} = 0.42$; Re = 5200. Oscillated front cylinder at the mean position (dir. $A'B'$).

Fig. 19. Typical flow pattern: $L/B = 3.50$, $T/B = 0$; $b/B = 1.5$, $(a/B)_{max} = 0.45$; Re = 5200. Oscillated front cylinder at the mean position (dir. $A'B'$).

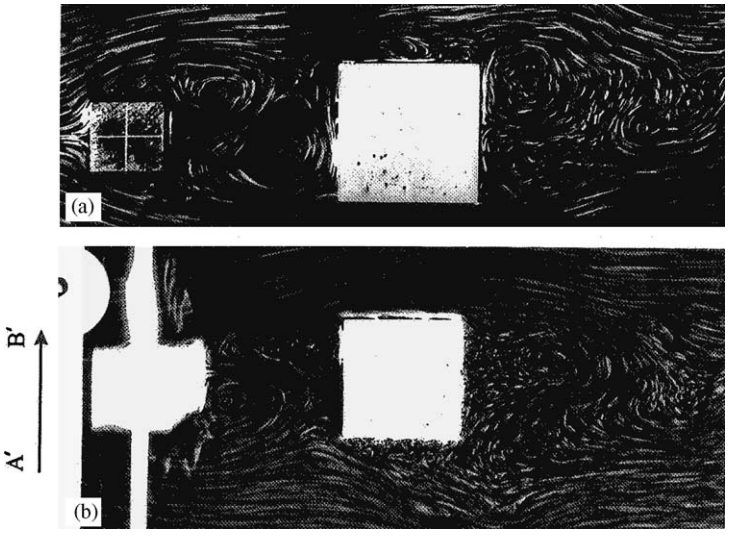

Fig. 20. Typical flow patterns: $L/B = 4.0$, $T/B = 0$; $b/B = 2.0$, $(a/B)_{max} = 0.50$; Re = 5200: (a) stationary cylinder and (b) oscillated front cylinder at the mean position (dir. $A'B'$).

Hence, in this case, the flow patterns obtained by using both a stationary and an oscillated front cylinder correspond with the vibratory response of the test cylinder.

The tandem location with $L/B = 2.0$ and $T/B = 0$ is an interesting one, where the effect of the b/B ratio on the vibratory amplitudes of the test cylinder can be clearly noticed. Fig. 21 shows the flow patterns at $b/B = 0.5$, 1.0, 1.5 and 2.0 for the square cylinder. Fig. 21(a) refers to the case of $b/B = 0.5$, where a vigorous shear layer rolling up process takes place around the front cylinder, indicating significant lift forces acting on it. This is reflected in the high response

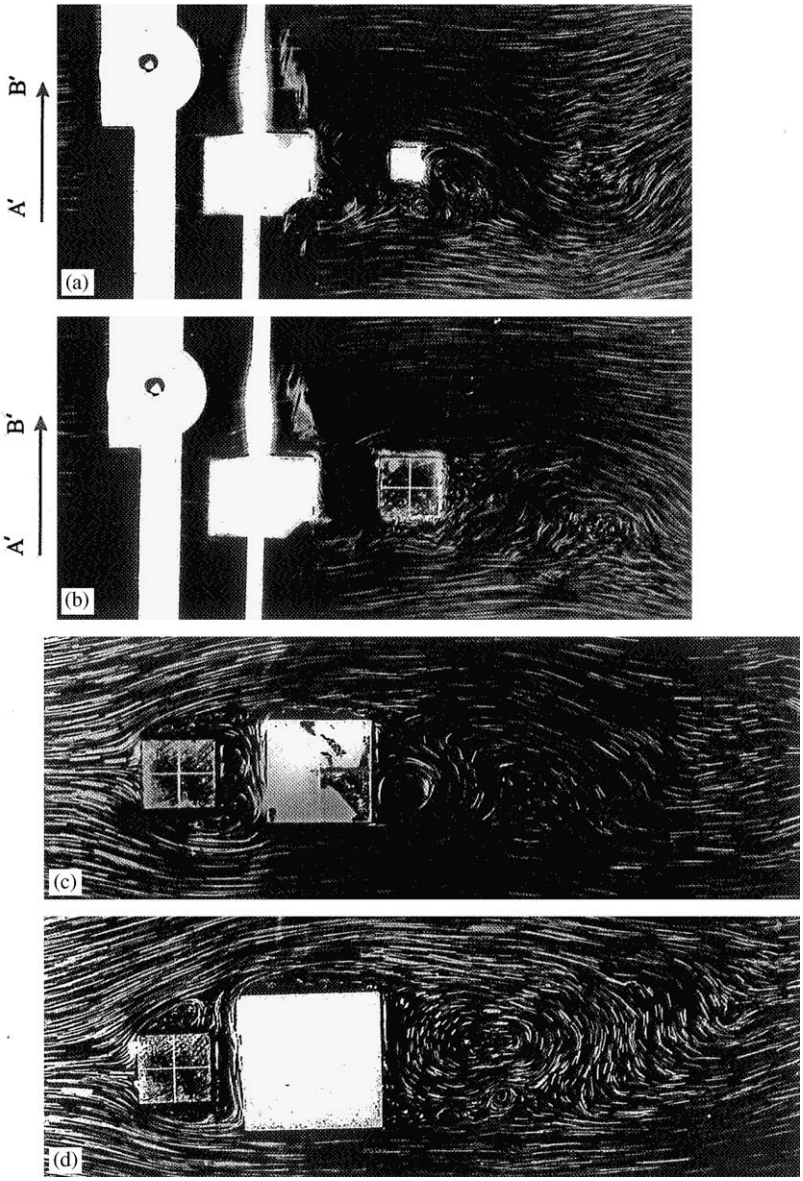

Fig. 21. Flow fields: $L/B = 2.0$, $T/B = 0$; Re = 5200: (a) $b/B = 0.5$, $(a/B)_{max} = 0.46$; (b) $b/B = 1.0$, $(a/B)_{max} = 0.40$; (c) $b/B = 1.5$, $(a/B)_{max} = 0.03$; (d) $b/B = 2.0$, $(a/B)_{max} = 0.02$. (a, b—oscillated front cylinder occupying mean position; c,d—front cylinder, stationary).

amplitude value observed for the test cylinder in air experiments ($(a/B)_{max} = 0.46$). Fig. 21(b) corresponds to $b/B = 1.0$, where the flow field seems to be similar to that of the case with $b/B = 0.5$, with regular vortex shedding taking place from the front cylinder. Correspondingly, it is observed that the test cylinder vibrates with considerably high amplitude in air experiments with $(a/B)_{max} = 0.40$.

For cases with $b/B = 1.5$ and 2.0, the vibratory amplitude observed in air experiments is negligibly small, with $(a/B)_{max} = 0.03$ and $(a/B)_{max} = 0.02$, respectively. Hence, flow-visualization experiments with a stationary test cylinder were performed, and the results are given in Fig. 21(c) and (d). Fig. 21(c) corresponds to $b/B = 1.5$ where it is seen that due to the presence of the bigger cylinder, strong cross-flow is induced in the gap between the cylinders, disrupting the shear layer roll-up process and thus the vortex shedding from the front cylinder. This is reflected in the substantially low

amplitude of vibration observed in this case, with $(a/B)_{max} = 0.03$ (Fig. 7(c)). Fig. 21(d) shows the flow pattern around the front cylinder for $b/B = 2.0$. In this case also, very strong cross-flow can be seen in the gap between the cylinders, disrupting the shear layers. This corresponds well with the substantially reduced amplitude of vibration of the test cylinder with $(a/B)_{max} = 0.02$ (Fig. 7(d)). Figs. 21(a)–(d) clearly shows the influence of size ratio (b/B ratio) on the flow-induced oscillations of the front cylinder due to the interference effects in a typical tandem arrangement.

3.2.2.2. Side-by-side arrangement. Flow-visualization results are obtained at some typical side-by-side arrangements when both cylinders are stationary and when one of them (lower) is oscillated. In all the photographs, the lower cylinder represents the test cylinder and upper one, the interfering cylinder. The maximum peak-to-peak amplitude is maintained the same as the corresponding value in the air experiments (Fig. 9). The other experimental details are the same as those described in Sections 2.2 and 3.2.2.

Figs. 22(a)–(c) shows the flow patterns around the oscillated lower cylinder occupying the mean vibratory position at $T/B = 2.0$ ($L/B = 0$). The results are presented for the b/B ratios of 0.5, 1.0 and 1.5 (for $b/B = 2.0$, the $(a/B)_{max}$ value is only 0.02, and hence the flow-visualization experiments with vibrated cylinder is not conducted). In this case also, for $b/B = 0.5$ (Fig. 22(a)), it can be seen that regular vortex shedding is taking place from the lower cylinder, indicating

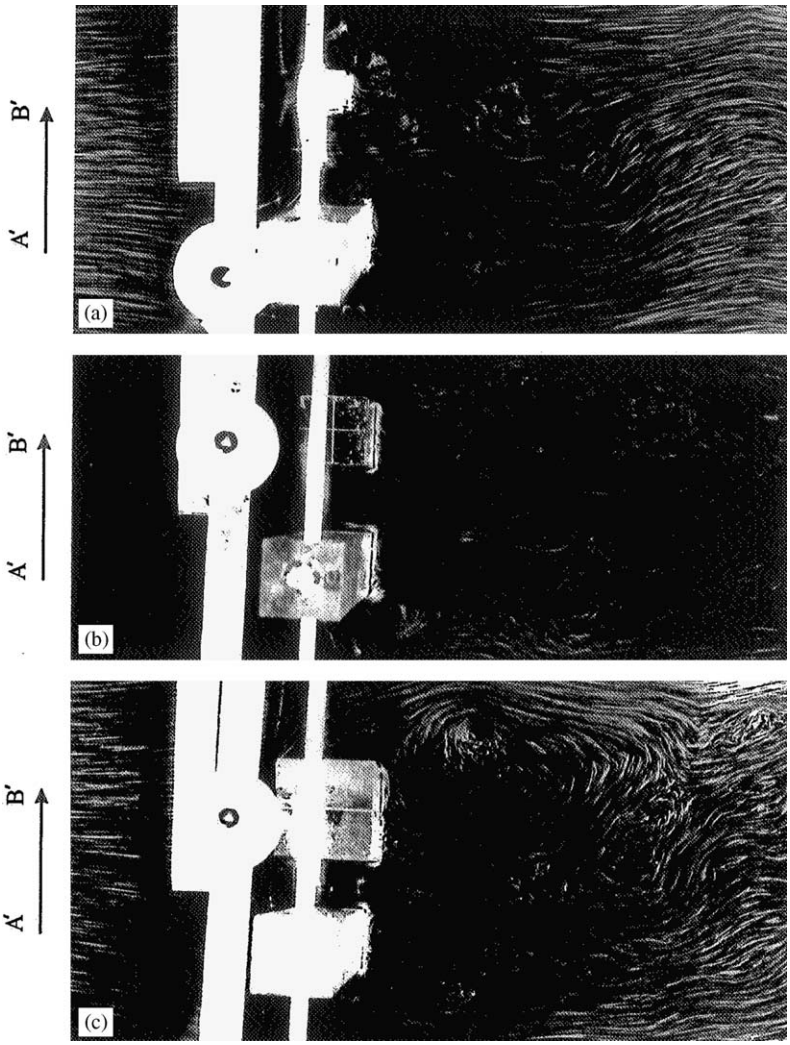

Fig. 22. Flow fields: $L/B = 0$, $T/B = 2.0$ (oscillated lower cylinder at the mean position; dir. $A'B'$): (a) $b/B = 0.5$, $(a/B)_{max} = 0.32$; (b) $b/B = 1.0$, $(a/B)_{max} = 0.12$; (c) $b/B = 1.5$, $(a/B)_{max} = 0.04$ and (d) $b/B = 2.0$, $(a/B)_{max} = 0.02$.

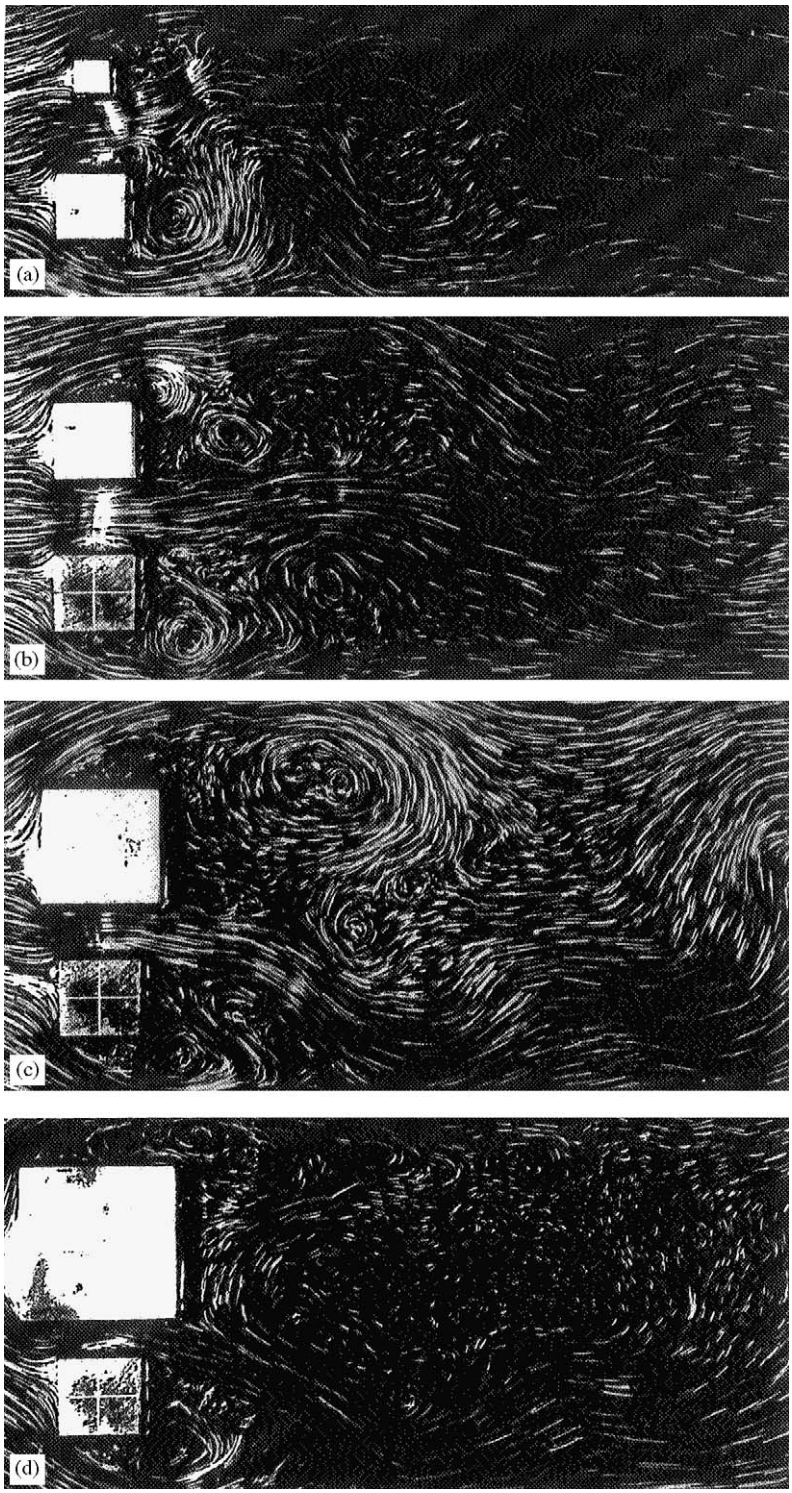

Fig. 23. Flow fields: $L/B = 0$, $T/B = 2.0$ (lower cylinder, stationary); Re = 5200. Other key details as in Fig. 22.

considerable periodic forces acting on it. As seen in Figs. 22(b)–(c), as the b/B ratio increases, the gap flow is becoming more and more biased towards the lower cylinder, disrupting the shear layer rolling up and thus the vortex shedding process. This indicates the possibility of a successive reduction in the lift force acting on the cylinder as the b/B ratio increases. This is reflected in the vibratory response amplitude values for $b/B = 1.0$ and 1.5, with $(a/B)_{max} = 0.12$ and 0.04, respectively.

At this location, flow-visualization experiments were conducted using a stationary lower cylinder also (Figs. 23(a)–(d)) for all the b/B ratios (= 0.5, 1.0,1.5 and 2.0). In this case also, as the b/B ratio increases, successive reduction of amplitudes could be inferred, due to similar flow field features as depicted in Fig. 22(a)–(d).

3.2.2.3. Staggered arrangement. Flow-visualization studies were conducted (both stationary and oscillated cases) at some typical staggered positions, and the results are presented and discussed in the following section. In the photographs presented, the upstream cylinder represents the test cylinder. The maximum peak-to-peak amplitude is maintained the same as in air experiments. The other experimental details are the same as those described in Sections 2.2 and 3.2.2. A large number of cases were photographed; however, only typical results are presented.

In Fig. 24 are shown the patterns around the upstream cylinder at a staggered location with $L/B = 3.0$ and $T/B = 1.25$, for $b/B = 1.0$. Fig. 24(a) refers to the case where the front cylinder occupies the mean vibratory position with direction of motion A' to B' (cylinder motion upwards). The flow field around the cylinder shows very vigorous

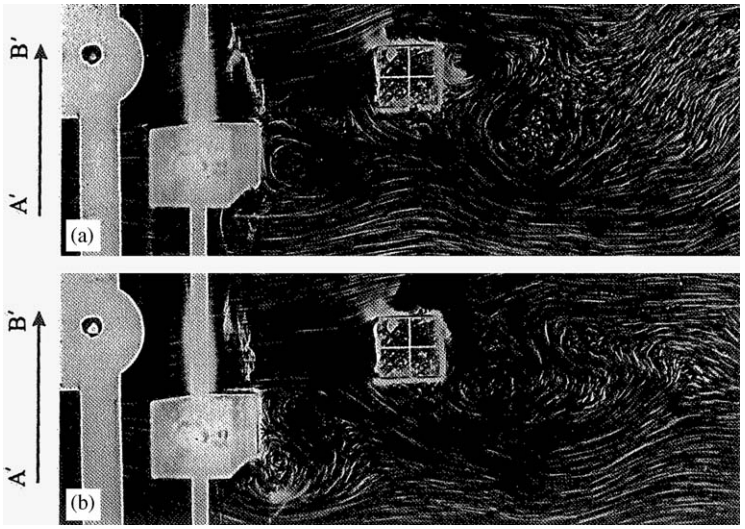

Fig. 24. Typical flow patterns: $L/B = 3.0$, $T/B = 1.25$; $b/B = 1.0$, $(a/B)_{max} = 0.43$; Re = 5200: (a) oscillated front cylinder at the mean position (dir. $A'B'$) and (b) oscillated front cylinder at an intermediate amplitude position ($a'/B = 0.07$ from the mean position; dir. $A'B'$).

Fig. 25. Typical flow pattern: $L/B = 4.0$, $T/B = 1.5$; $b/B = 2.0$, $(a/B)_{max} = 0.47$; Re = 5200. Oscillated front cylinder at the mean position (dir. $A'B'$).

rolling up of shear layers, which can contribute to a significant lift force acting on it. Fig. 24(b) refers to the case where the front cylinder occupies another vibratory position in its oscillatory path with $a'/B = 0.07$ and corresponds to the same direction of motion as at Fig. 24(a). In this case also (Fig. 24(b)), vigorous vortex shedding similar to that shown in Fig. 24(a) is seen, substantiating the vibratory amplitude observed ($(a/B)_{max} = 0.43$; Fig. 11(b)).

Fig. 25 shows the flow patterns at $L/B = 4.0$ and $T/B = 1.5$, for $b/B = 2.0$. At this position, the test cylinder in air experiments exhibits significant amplitude of vibration with $(a/B)_{max} = 0.47$ (Fig. 13(a)). In Fig. 25, the test cylinder is at the mean vibratory position, where it could be seen that the presence of interfering cylinder strengthens the vortex shedding process from the front cylinder (see also Fig. 16(b)) which can contribute to significant lift forces to act on it. As can be seen, the flow-visualization results do give a considerable physical explanation in understanding the vibratory response of the test cylinder.

With regard to the multiple amplitude of motion which the test cylinder has executed in isolated as well as in all the cases with interference, it should be pointed out that further flow-visualization results, with an oscillated cylinder undergoing or forced to undergo similar multiple amplitudes of motion (as in the air experiments) in a water channel or flow visualization in a wind tunnel when the test cylinder is vibrating, would give better insight in to the physics of cylinder motion.

4. Concluding remarks

From the investigations carried out, the following conclusions are drawn.

(i) Unlike a circular cylinder, a square cylinder exhibits multiple amplitudes within a low and a high peak in the entire resonance range of the single cylinder response. Compared to a circular cylinder, a square cylinder has got a wider lock-in range and a higher (and also a flatter) peak amplitude of vibration. The square cylinder was found to exhibit multiple amplitudes in all the cases of interference also.

(ii) With interference, the oscillatory amplitude was found to depend on the relative dimensions, the transverse and longitudinal spacing between the cylinders and also on the body geometry. Accordingly, there could be magnification or suppression of vibratory amplitudes. Under identical conditions, in general, the square cylinder was found to exhibit higher amplitudes of vibration than the circular cylinder.

(iii) Among the arrangements tested, the tandem arrangement was found to give rise to maximum magnification of vibratory amplitudes. The higher the b/B ratio, the larger was found to be the longitudinal spacing at which the peak amplitude occurs.

(iv) The flow-visualization results obtained explain the vibratory response of the test cylinder in most of the cases.

(v) The flow-visualization results presented have a limitation with respect to explaining the multiple amplitude of vibration of the isolated test cylinder as well as in the cases with interference. Either flow-visualization experiments in the wind tunnel itself when the test cylinder is vibrating, or flow-visualization experiments in a water channel with the cylinder oscillated simulating the multiple amplitude of vibration, are required to get more insight into the physics involved, and then to provide a concrete explanation.

References

Bailey, P.A., Kwok, K.C.S., 1985. Interference excitation of twin tall buildings. Journal of Wind Engineering and Industrial Aerodynamics 21, 323–338.

Bearman, P.W., Luo, S.C., 1988. Investigation of the aerodynamic instability of a square-section cylinder by forced oscillation. Journal of Fluids and Structures 2, 161–176.

Bearman, P.W., Obasaju, E.D., 1982. An experimental study of pressure fluctuations on fixed and oscillating square section cylinders. Journal of Fluid Mechanics 119, 297–321.

Bearman, P.W., Gartshore, I.S., Maull, D.J., Parkinson, G.V., 1987. Experiments on flow-induced vibration of a square section cylinder. Journal of Fluids and Structures 1, 19–34.

Bishop, R.E.D., Hassan, A.Y., 1964. The lift and drag forces on a circular cylinder in a flowing fluid. Proceedings of the Royal Society of London Series A 277, 32–50.

Blessmann, J., Riera, J.D., 1985. Wind excitation of neighbouring tall buildings. Journal of Wind Engineering and Industrial Aerodynamics 18, 91–103.

Bokaian, A., Geoola, F., 1985. Wake displacement as cause of lift force on cylinder pair. ASCE Journal of Engineering Mechanics 111, 92–99.

Bostok, B.R., Mair, W.A., 1972. Pressure distributions and forces on rectangular and D-shaped cylinders. Aeronautical Quarterly 23, 1–6.

Gowda, B.H.L., Deshkulkarni, K.P., 1988. Interference effects on the flow-induced vibrations of a circular cylinder in side-by-side and staggered arrangement. Journal of Sound and Vibration 122, 465–478.

Gowda, B.H.L., Prabhu, D.R., 1987. Interference effects on the flow-induced vibrations of a circular cylinder. Journal of Sound and Vibration 112, 487–502.

Gowda, B.H.L., Sreedharan, V., 1994. Flow-induced oscillations of a circular cylinder due to interference effects. Journal of Sound and Vibration 176, 497–514.

Laneville, A., Lu, Z., 1983. Mean flow patterns around two dimensional rectangular cylinders and their interpretation. Journal of Wind Engineering and Industrial Aerodynamics 14, 387–398.

Luo, S.C., Teng, T.C., 1990. Aerodynamic forces on a square section cylinder that is downstream to an identical cylinder. Aeronautical Journal 94, 203–212.

Luo, S.C., Yazdani, Md., G., Chew, Y.T., Lee, T.S., 1994. Effects of incidence and after body shape on flow past bluff cylinders. Journal of Wind Engineering and Industrial Aerodynamics 53, 375–399.

Lyn, D.A., Einav, S., Rodi, W., Park., J.H., 1995. A laser-Doppler velocimetry study of ensemble-averaged characteristics of the turbulent near wake of a square cylinder. Journal of Fluid Mechanics 304, 285–319.

Nakamura, Y., Mizota, T., 1975. Unsteady lifts and wakes of oscillating rectangular prisms. ASCE Journal of Engineering Mechanics Division 101, 855–871.

Obasaju, E.D., 1983. An investigation of the effects of incidence on the flow around a square section cylinder. Aeronautical Quarterly 34, 243–259.

Okajima, A., 1990. Numerical simulation of flow around rectangular cylinders. Journal of Wind Engineering and Industrial Aerodynamics 33, 171–180.

Olivari, D., 1983. An investigation of vortex shedding and galloping induced oscillation on prismatic bodies. Journal of Wind Engineering and Industrial Aerodynamics 11, 307–319.

Parkinson, G.V., 1971. Wind-induced instability of structures. Philosophical Transactions of the Royal Society of London Series A 269, 395–409.

Sakamoto, H., Haniu, H., 1988. Aerodynamic forces acting on two square prisms placed vertically in a turbulent boundary layer. Journal of Wind Engineering and Industrial Aerodynamics 31, 41–66.

Sakamoto, H., Haniu, H., Obata, Y., 1987. Fluctuating forces acting on two square prisms in a tandem arrangement. Journal of Wind Engineering and Industrial Aerodynamics 26, 85–103.

Shiraishi, N., Matsumoto, M., Shirato, H., 1986. On aerodynamic instabilities of tandem structures. Journal of Wind Engineering and Industrial Aerodynamics 23, 437–447.

Sreedharan, V., 1992. Interference effects on the flow induced oscillations of a circular cylinder. M.S. Thesis, Indian Institute of Technology Madras, Chennai, India.

Takeuchi, T., 1990. Effects of geometrical shape on vortex-induced oscillations of bridge tower. Journal of Wind Engineering and Industrial Aerodynamics 33, 359–368.

Takeuchi, T., Matsumoto, M., 1992. Aerodynamic response characteristics of rectangular cylinders in tandem arrangement. Journal of Wind Engineering and Industrial Aerodynamics 41–44, 565–575.

Takeuchi, T., Matsumoto, M., 1993. Vortex-induced oscillations of tandem rectangular bluff bodies. Journal of Wind Engineering and Industrial Aerodynamics 45, 421–430.

Taniike, Y., 1992. Interference mechanism for enhanced wind forces on neighbouring tall buildings. Journal of Wind Engineering and Industrial Aerodynamics 41–44, 1073–1083.

Taniike, Y., Inaoka, H., 1988. Aeroelastic behaviour of tall buildings in wakes. Journal of Wind Engineering and Industrial Aerodynamics 28, 317–327.

Vickery, B.J., 1966. Fluctuating lift and drag on a long cylinder of square cross-section in a smooth and in a turbulent stream. Journal of Fluid Mechanics 25, 481–494.

Wilkinson, R.H., 1981. Fluctuating pressures on an oscillating square prism. Aeronautical Quarterly 32, 97–110.

Zdravkovich, M.M., 1985. Flow induced oscillations of two interfering circular cylinders. Journal of Sound and Vibration 101, 511–521.